Effect of stress on the energy levels of the vacancy-oxygen-hydrogen complex in Si

J. Coutinho*
Department of Physics, University of Aveiro, 3810 Aveiro, Portugal
and School of Physics, University of Exeter, Stocker Road, Exeter EX4 4QL, United Kingdom

O. Andersen†
Center for Electronic Materials, Devices and Nanostructures, University of Manchester Institute of Science and Technology, P.O. Box 88, Manchester M60 1QD, United Kingdom
and Institute of Physics and Astronomy, University of Aarhus, Ny Munkegade, DK-8000 Aarhus C, Denmark

L. Dobaczewski
Institute of Physics, Polish Academy of Sciences, al. Lotników 32/46, 02-668 Warsaw, Poland

K. Bonde Nielsen
Institute of Physics and Astronomy, University of Aarhus, Ny Munkegade, DK-8000 Aarhus C, Denmark

A. R. Peaker
Center for Electronic Materials, Devices and Nanostructures, University of Manchester Institute of Science and Technology, P.O. Box 88, Manchester M60 1QD, United Kingdom

R. Jones
School of Physics, University of Exeter, Stocker Road, Exeter EX4 4QL, United Kingdom

S. Öberg
Department of Mathematics, Luleå University of Technology, Luleå S-97187, Sweden

P. R. Briddon
School of Natural Sciences, University of Newcastle upon Tyne, Newcastle upon Tyne NE1 7RU, United Kingdom
(Received 24 June 2003; published 18 November 2003)

The piezospectroscopic properties of the *V*OH defect in Si are found using stress Laplace deep level transient spectroscopy (DLTS) and are compared with local density-functional calculations of (i) the acceptor level and its shift under stress, and (ii) the alignment of the neutral center under stress. The theory is able to account for two acceptor levels observed for ⟨100⟩, ⟨111⟩, and ⟨110⟩ stress even though additional splitting is expected for a defect with static C_{1h} symmetry. This is related to (i) a rapid reorientation of the H atom within the defect at temperatures at which the DLTS experiments are carried out, and (ii) the small effect of stress on two orientations of the defect under ⟨110⟩ stress. The theory is also able to give a quantitative account of the alignment of the center. The effect of stress on the reorientation barrier of the defect is also investigated. The reorientation barrier of the defect in its positive charge state is found theoretically to be very small, consistent with the lack of any splitting in the donor level under stress.

DOI: 10.1103/PhysRevB.68.184106 PACS number(s): 61.72.Bb, 61.72.Ji, 68.55.Ln, 71.55.Cn

I. INTRODUCTION

Low-temperature electron-irradiation of Si crystals introduces vacancies and self-interstitials, neither of which are stable as isolated defects at room temperature. They diffuse and are trapped by impurities such as oxygen.[1] The vacancy-oxygen, *V*O, center[2] is a well-known and well-understood defect which is stable up to ~300 °C.[3] The oxygen atom passivates two of the Si dangling bonds and the electrical activity of the center comes from a weakly reconstructed Si-Si bond bridging the remaining Si neighbors bordering the vacancy. This bond is associated with an acceptor level at $E_c - 0.17$ eV. Hydrogen, often unintentionally introduced during growth or processing, readily reacts with the reconstructed bond leading to the formation of *V*OH and VOH_2 defects. The latter is electrically inactive but has been detected in infrared absorption studies.[4] The former defect is electrically active and has been suggested to possess acceptor and donor levels at $E_c - 0.31$ eV and $E_v + 0.28$ eV, respectively.[5–8] When neutral, it is a $S = 1/2$ center that has been observed in electron-paramagnetic-resonance (EPR) experiments.[9] Here, it was established that it possessed monoclinic-I (C_{1h}) symmetry below ~180 K, but above 240 K it exhibits an apparent orthorhombic-I (C_{2v}) symmetry due to the H atom jumping between the two Si dangling bonds with an activation energy of ~0.18 eV. The defect anneals out around 300 °C.[9]

Previous theoretical calculations have been made on the structure[10] and local vibrational modes of *V*OH.[11] According to these calculations, both O and H atoms lie inside the va-

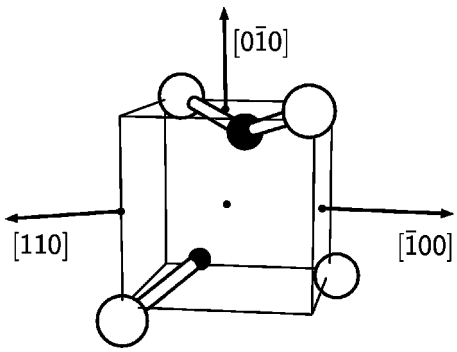

FIG. 1. Model for the *V*OH defect in silicon. Silicon, oxygen, and hydrogen atoms are represented as white, large black, and small black spheres, respectively. Each Si atom is bonded to three more Si atoms not depicted in the figure.

cant site as shown in Fig. 1. The O atom bridges two second neighbor Si atoms while H passivates a third Si dangling bond leaving a single remaining unsatisfied Si radical. However, the electrical properties of the center have not been investigated by theory in detail, and this is one of the aims of the present paper.

A comprehensive piezospectroscopic study of the *V*O complex employing Laplace deep level transient spectroscopy (LDLTS) together with an uniaxial stress has recently been reported by Dobaczewski *et al.*[12] In this work, the authors not only confirmed the previously measured defect-host coupling character (in the form of a stress tensor B),[2] but they also investigated the effect of stress on the saddle-point structure for defect reorientation. They concluded that at this saddle point, the defect possessed trigonal symmetry implying that the oxygen atom lies along $\langle 111 \rangle$ and is bonded to three Si atoms. This has given an original insight into the behavior of a moving defect and presents a challenge for theoretical work.

In this paper we report a combined experimental and theoretical study of the singly hydrogenated *V*O complex (*V*OH). We employ DLTS, high-resolution LDLTS[13] in combination with uniaxial stress, and total-energy *ab initio* calculations to produce a detailed model consistent with the measured dynamical, electrical, and piezospectroscopic data.

II. SAMPLE PREPARATION

The samples used for this work were prepared from $\{110\}$ oriented Czochralski grown *n*-type and *p*-type silicon wafers of resistivity 20Ω cm. The wafers were cut into shapes of $\sim 7 \times 2 \times 1$ mm^3 bars with the long edge parallel to one of the major crystallographic directions, $\langle 100 \rangle$, $\langle 110 \rangle$, and $\langle 111 \rangle$. A $\{111\}$ oriented float-zone *n*-type silicon wafer of resistivity 38–50Ω cm was also used for zero-stress measurements. The *V*OH complexes were formed either by implantation of protons or by irradiation of electrons followed by remote hydrogen plasma treatment. Implantations were carried out with protons of energy ~400 keV to a dose of $\sim 1 \times 10^{10}$ cm^{-2}. Irradiations were carried out with electrons of energy ~2 MeV to a dose of $\sim 5 \times 10^{14}$ cm^{-2}. Details of the setup used for implantations and irradiations are given elsewhere.[14] The system used for remote plasma treatments consisted of a quartz tube through which a molecular hydrogen gas at a pressure of ~1.0 mbar was pumped. The plasma was excited by a 13.56-MHz generator connected to a copper coil encircling the tube. The samples were located in a remote position to the plasma in order to minimize damage due to ion bombardment. Treatments were carried out in the temperature range of 30–120 °C at a power of ~30 W for typically 60 min. Schottky diodes and Ohmic contacts were formed on *n*-type silicon by evaporation of gold (or platinum) and aluminum, respectively. For *p*-type samples the Schottky diodes and Ohmic contacts were formed by sputtering of titanium and evaporation of gold, respectively.

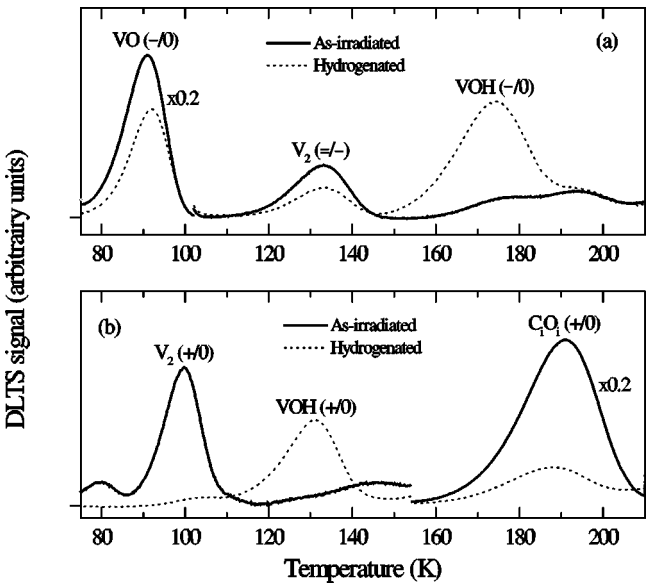

FIG. 2. (a) 200 s^{-1} conventional DLTS spectra of as-irradiated and irradiated hydrogenated *n*-type silicon. The plasma treatment was carried out for 20 min at 30 °C. (b) 50 s^{-1} conventional DLTS spectra of as-irradiated and irradiated, hydrogenated *p*-type silicon. The plasma treatment was carried out for 60 min at 120 °C.

III. EXPERIMENTAL RESULTS

Figure 2(a) shows conventional DLTS spectra of as-irradiated and irradiated, plasma treated *n*-type silicon. In the as-irradiated and irradiated, hydrogen plasma treated material, the spectra are dominated by the well-known peaks related to the single acceptor level of the vacancy-oxygen complex, VO$(-/0)$, and the double acceptor level of the divacancy, $V_2(=/-)$.[15,16] After hydrogenation, the intensities of these peaks are significantly reduced and a hydrogen-related peak appears at ~175 K. This peak is also observed in the proton implanted samples. The Arrhenius plots for the electron emission processes are practically indistinguishable in the irradiated, hydrogenated material and the implanted material, confirming that the levels are identical. In both cases, the activation enthalpy is obtained as $\Delta H_n = 0.31$ eV. We have previously identified the level at $E_c - 0.31$ eV as the acceptor level of the *V*O complex saturated by a single hydrogen atom, *V*OH$(-/0)$.[6,7] The results of the

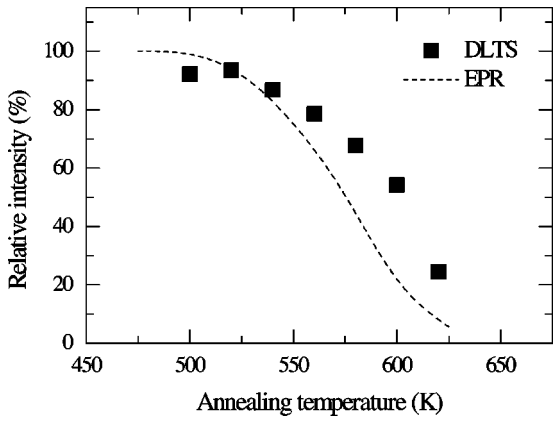

FIG. 3. Correlation of Laplace DLTS and EPR (Ref. 9) isochronal annealing data of the *V*OH complex. The intensities were normalized to the values obtained before annealing. The EPR data have been shifted slightly in temperature to comply with our 60 min annealing time.

present work are fully consistent with this interpretation.

The *V*OH complexes are formed as a product of the interaction of diffusing atomic hydrogen with immobile *V*O complexes generated by the irradiation. In general, however, the increase in the concentration of the *V*OH complexes after hydrogenation is significantly smaller than the corresponding decrease in the concentration of the *V*O complexes. After strong hydrogenation, the sum signal of *V*O and *V*OH is decreased by more than 70%. No other defect with an obvious link to the *V*O complex are observed in the DLTS spectra. This loss of electrically active defects after hydrogenation is likely due to the formation of the fully saturated *V*O complex containing two hydrogen atoms, i.e., the VOH_2 structure which is formed in regions with high hydrogen content and is electrically inactive.[4]

Comparison of annealing data is one of the most efficient tools to establish a correlation between defects observed by different experimental techniques. In the present work, we have carried out isochronal annealing of the *V*OH complex and compared the results with those from EPR data.[9] Heat treatments were carried out for periods of 60 min in a nitrogen flow furnace. After each annealing step, the concentration of *V*OH(−/0) was measured by Laplace DLTS at a temperature of 162 K. Figure 3 depicts the relative intensity of *V*OH as a function of annealing temperature. A clear correlation exists between our Laplace DLTS results (squares) and the corresponding EPR data (smoothed curve). The absolute transition temperatures agree well considering the fact that the dose regimes of the two experimental techniques differ by more than three orders of magnitude. The isochronal annealing data were analyzed using an Arrhenius plot. Assuming a preexponential frequency of $\sim 10^{13}\ s^{-1}$, we conclude that the disappearance of *V*OH is mediated by a $\sim$2-eV barrier.

Figure 2(b) shows conventional DLTS spectra of as-irradiated and irradiated, hydrogen plasma treated *p*-type silicon. The spectra obtained after irradiation are dominated by the peaks related to the donor level of the divacancy V_2 (Ref. 17) and the donor level of the interstitial carbon-oxygen complex C_iO_i.[18] As in the case of *n*-type material, the concentrations of the radiation induced defects are strongly reduced by hydrogenation. Further, a hydrogen-related peak appears at $\sim$130 K. The activation enthalpy for the hole emission from this level is obtained as $\Delta H_p = 0.26$ eV. Recently, a similar level formed by chemical etching of irradiated *p*-type silicon was related to the donor level of the *V*OH complex.[8] This conclusion is supported by earlier observations of similar annealing behavior of the traps with levels located at $E_c - 0.31$ eV and $E_v + 0.26$ eV.[5] The results of the present work are consistent with the above interpretation. As reported in Ref. 8, we did not observe the $E_v + 0.26$ eV trap in the hydrogenated *p*-type samples, unless reverse bias annealing is performed. This effect was attributed to the high efficiency of hydrogen trapping by B acceptors, with the formation of *V*OH complexes taking place only after B-H defects anneal out.

A. Introduction to the stress measurements

In the absence of external perturbations, an anisotropic point defect in Si is found randomly aligned with a maximum of 24 possible orientations allowed by the symmetry of the host. Under uniaxial stress, given by an axial tensor σ, only 12 out of these 24 alignments are distinguishable. Each orientation is degenerate in the sense that all defects have the same free energy of formation G_0. For a specific orientation *i*, charge state *q*, and applied strain ϵ, the defect energy change is given by $\Delta^{iq} = G^{iq} - G_0^q = \mathrm{Tr}[B^{iq} \cdot \epsilon]$, where B^{iq} is a stress-energy tensor associated with the defect in charge state *q* aligned along *i*.[19–21] Similarly, we can express Δ^{iq} as a response to an external uniaxial stress *P* (defined to be negative for compression), along the unit vector **t**. Given the related stress tensor as $\sigma_{kl} = t_k t_l P$, we have $\Delta^{iq} = \Sigma_{klmn} B_{kl}^{iq} \cdot s_{klmn} \cdot t_m t_n \cdot P$, where s_{klmn} are the compliance constants of the host material.

From the experimental point of view, it is convenient to contract *B* and *s* by introducing a strain coefficient α_t^{iq} which is related to a defect orientation *i* under stress along *t*, i.e.,

$$\Delta_t^{iq} = B_{kl}^{iq} \cdot s_{klmn} \cdot t_m t_n \cdot P = \alpha_t^{iq} P, \tag{1}$$

where we note that α_t^{iq} is associated with a specific charge state *q* of the defect. For example, for a monoclinic-I (C_{1h}) defect in a cubic host we expect that under $\langle 100 \rangle$ compressive stress, the defects will split into two populations with energies shifted at a rate

$$\alpha_{100}^{1q} = -2B_{xx}^q (s_{11} - s_{12}), \qquad \alpha_{100}^{2q} = B_{xx}^q (s_{11} - s_{12}),$$

where we utilize the Voigt symmetrized form of *s*. The population splitting ratio is 4:8, and observations of the number of and magnitude of populations provides us with information on the symmetry of the defect and α^{iq} gives information on the tensile or compressive nature of the defect along a specific direction. For example, if $\alpha_{100}^{iq} < 0$ the alignment *i* is compressive along [100]. Since the energy shifts depend on charge state *q*, the thermodynamic energy level, as determined in a DLTS experiment, where the stress dependence of the preexponential factor has been taken into account, will be

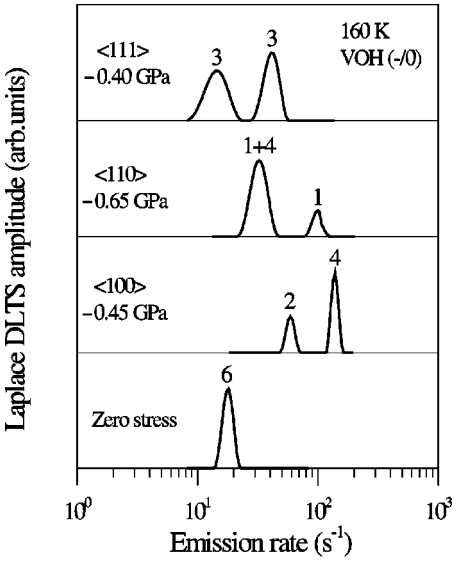

FIG. 4. Laplace DLTS spectra of VOH$(-/0)$ recorded at 160 K at zero stress and under uniaxial stress along the three major crystallographic directions. The amplitude of the zero-stress peak has been normalized to a value of 6 units. The splitting pattern establishes the effective orthorhombic-I C_{2v} symmetry of the defect.

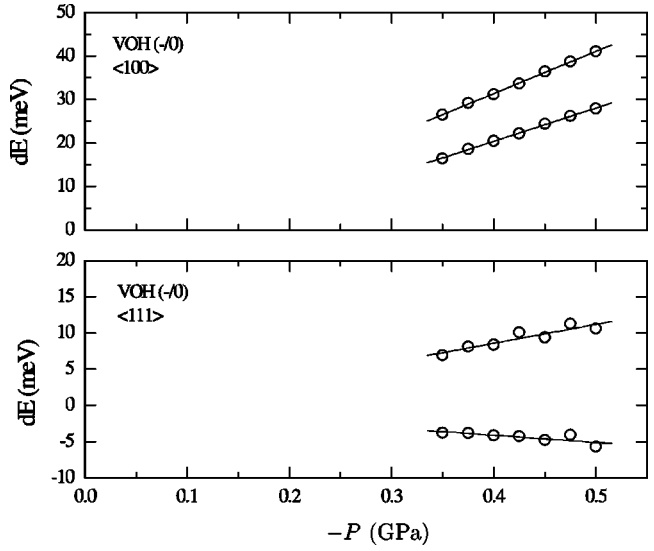

FIG. 5. Energy shifts versus applied stress for the split lines of VOH$(-/0)$ under stress along the $\langle 100\rangle$ and $\langle 111\rangle$ directions. The energy shifts have been obtained as $dE = k\,T\ln[e_n(P)/e_n(0)]$, where $T = 155$ K is the measurement temperature and $e_n(P)$ is the directly measured electron emission rate at the given stress. A positive slope means that the energy level approaches the conduction band under stress. The line splittings are obtained as 21 meV/GPa for the $\langle 100\rangle$ stress direction and 36 meV/GPa for the $\langle 111\rangle$ stress direction.

different for the different populations and a splitting of the energy level will be observed. The splitting of the $(-/0)$ level of the defect is given by the differences in $\alpha_{100}^{i0} - \alpha_{100}^{i-}$, denoted by $\alpha_{100}^{i(-/0)}$, among different i. This is the case provided that the defect is not able to jump rapidly between different orientations in the time scale of the experiment. When measurements take place at temperatures at which the defect is able to jump rapidly between, say, two orientations, only one line is expected from the pair of orientations and the observed transition then corresponds to the orientation having the smaller ionization energy.

The intensities of the DLTS lines reflect the numbers of centers in the different populations. If the centers are introduced in the absence of stress, no particular orientation is favored and they are in a condition of random alignment. If stress is then applied at a temperature where they cannot reorientate, then the DLTS amplitudes will reflect the number of equivalent orientations allowed by symmetry.

However, when reorientation can take place under stress, and an equilibrium is established among the populations for a given charge state q, a condition called alignment takes place. If the sample is then quenched, the populations will be frozen and the relative intensities of the different DLTS lines reflect a Boltzmann distribution dependent on the temperature at which reorientation occurred, and the energy differences, given by Δ_t^{iq}, between the populations in the stress field.

B. Stress-splitting experiments

Figure 4 shows the Laplace DLTS spectra of VOH$(-/0)$ recorded at 160 K at zero stress and under uniaxial stress along the three major crystallographic directions. For each direction, the zero-stress peak splits into two components. The amplitudes of the split lines sum up to the amplitude of the zero-stress peak. Within experimental error, the relative amplitudes of the individual peaks in Fig. 4 agree with the ratios expected for a defect of orthorhombic-I symmetry, i.e., 2:4 for the $\langle 100\rangle$ stress direction, $(1+4)$:1 for the $\langle 110\rangle$ stress direction and 3:3 for the $\langle 111\rangle$ stress direction. The splitting of the $(1+4)$ component expected for $\langle 110\rangle$ stress is unresolved.

The apparent orthorhombic-I C_{2v} symmetry of the defect is related to a partial thermal averaging effect discussed in Sec. III A. As established by EPR measurements,[9] the hydrogen atom swiftly jumps between equivalent sites in the $\{110\}$ mirror plane of the VOH defect. The O atom cannot jump at these temperatures. The hydrogen jump rate is much larger than the rate of the electron ionization process monitored in the Laplace DLTS measurements, by approximately five orders of magnitude at the measurement temperature. Consequently, the static monoclinic-I C_{1h} symmetry is changed to an effective orthorhombic-I C_{2v} symmetry under the given experimental conditions, in agreement with the observed splitting pattern. This effect is discussed in detail below.

We have studied the influence of uniaxial stress on the ionization process $V\mathrm{OH}^- \rightarrow V\mathrm{OH}^0 + e^-$ by recording the emission rates of the split lines at different stress intensities at a fixed temperature. Figure 5 depicts the energy shifts versus stress amplitude for the split lines in the $\langle 100\rangle$ and $\langle 111\rangle$ stress directions. For both directions of stress, the data are consistent with a linear splitting. As in stress-splitting experiments we probe both neutral and negative charge states, and we shall write the splittings as the differences between the strain coefficients. Hence we get

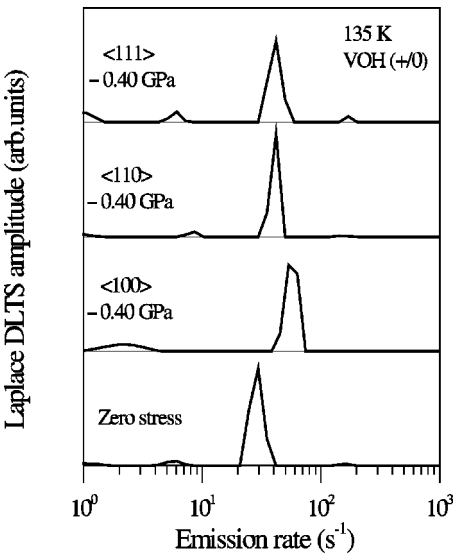

FIG. 6. Laplace DLTS spectra of VOH(0/+) recorded at 135 K at zero stress and under $P=-0.40$ GPa stress along the three major crystallographic directions.

$$\alpha_{100}^{f(-/0)}-\alpha_{100}^{s(-/0)}=21 \text{ meV/GPa},$$

$$\alpha_{111}^{f(-/0)}-\alpha_{111}^{s(-/0)}=36 \text{ meV/GPa},$$

where the superscripts f and s label the two populations and stand for the fast (or high-frequency) and slow (or low-frequency) emitting defects, respectively. The splitting of the two lines in the $\langle 110\rangle$ stress direction requires very high stresses and it is extremely difficult to determine a reliable strain coefficient. We estimate that the rate of splitting is approximately

$$\alpha_{110}^{f(-/0)}-\alpha_{110}^{s(-/0)}\sim 20 \text{ meV/GPa}.$$

The data in Fig. 5 show that the two lines in the $\langle 100\rangle$ stress direction do not converge to zero energy at zero stress. This indicates a nonlinearity of the splitting data at lower stresses. Recently, we observed a comparable effect for the acceptor level of the VO complex and established that the nonlinearity is related to a stress dependence of the electron-capture process in the $\langle 100\rangle$ stress direction.[12] In the present case of VOH$(-/0)$, it is not possible to measure directly the splitting curve and examine the capture process at lower stresses as the line splitting is below the energy resolution in this stress range. However, from the analogy with the VO complex, we propose that the lack of convergence in the $\langle 100\rangle$ stress direction is related to a stress dependence of the capture process for this particular direction of stress. Nevertheless, it is important to emphasize that the linear splitting in the high-stress regime is independent of the capture process, and the high-temperature slopes are true measures of energy shifts.

The donor level VOH(0/+) has also been studied by uniaxial stress in combination with Laplace DLTS. Figure 6 depicts Laplace DLTS spectra recorded at 135 K at zero stress and under -0.40 GPa stress applied along the three major crystallographic directions. No line splitting or peak broadening is observed for any of the stress directions. These conclusions were confirmed at a number of temperatures and for stresses up to about -0.50 GPa. For all directions of stress, the level approaches the valence band linearly with the applied stress. The lack of line splitting suggests that the effective symmetry of the initial charge state of the defect is cubic. The cubic symmetry can arise from either (i) a defect with a true static cubic symmetry or (ii) a defect of lower symmetry which displays an effective cubic symmetry due to thermal averaging at the measurement temperature. The first explanation is not consistent with a VOH defect. The latter explanation requires that the reorientation rate of the defect, determined by the jump rates of oxygen and hydrogen, is much higher than the ionization rate at the measurement temperature, and therefore the reorientation barrier of the whole defect should be less than 0.3 eV. Below, we shall show that the positively charged defect $(V\text{OH})^+$ has relatively small reorientation barriers for oxygen and hydrogen, and thus the effective cubic symmetry class is consistent with the VOH donor level.

C. Stress-alignment experiments

Stress-induced alignment experiments on the neutral defect have been carried out for the $\langle 100\rangle$ and $\langle 111\rangle$ stress directions. In both cases a significant effect of alignment was observed at temperatures above ~ 200 K when both O and H are able to jump. The equilibrium distribution between nonequivalent orientations was reached by applying the stress for approximately 15 min at 221 K for the $\langle 100\rangle$ stress direction and 225 K for the $\langle 111\rangle$ stress direction. Subsequently, the sample was cooled quickly to the measurement temperature and the occupancy ratio of defects in nonequivalent orientations was evaluated from the corresponding Laplace DLTS peaks. In all cases it was confirmed experimentally that a steady-state condition was reached. The VOH complexes were kept in the neutral charge state by applying a reverse bias during alignment.

Figure 7 shows examples of Laplace DLTS spectra after alignment at different stresses along $\langle 111\rangle$. The data demonstrate that the population of centers responsible for the high-frequency transition, i.e., the smaller ionization energy, decreases as a function of stress. In contrast, Fig. 8 shows that the amplitude ratio of the low-frequency line to the high-frequency line decreases with stress along $\langle 100\rangle$. For both directions of stress, the sum of the amplitudes of the split lines is independent of stress and equal to the zero-stress amplitude. The data are well described by Boltzmann statistics and lead to the strain coefficients $\alpha_{100}^{f0}-\alpha_{100}^{s0}=+109$ meV/GPa for the $\langle 100\rangle$ stress direction and $\alpha_{111}^{f0}-\alpha_{111}^{s0}=-108$ meV/GPa for the $\langle 111\rangle$ stress direction. In Sec. IV we give a detailed interpretation of the splitting and alignment data.

Due to the temperature at which the measurements are taken, the *frozen* C_{1h} structure cannot be measured. However, we can still study the remaining degree of freedom corresponding to the reorientation of the O atom. The stress-induced variation of the reorientation barrier ΔE_r separating the two s and f orientations of $V\text{OH}^0$ was measured. This

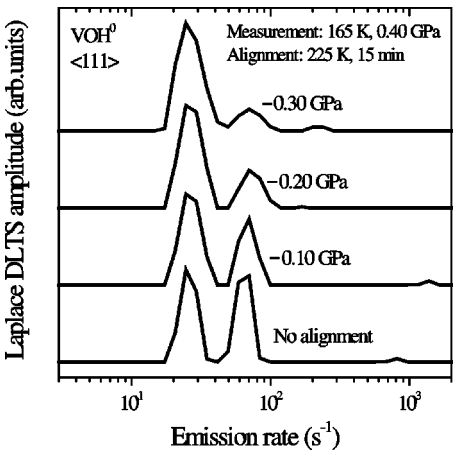

FIG. 7. Laplace DLTS spectra of *V*OH(−/0) obtained at 165 K under −0.40 GPa stress along the ⟨111⟩ direction. The spectra have been recorded after 15 min alignment of the neutral defect *V*OH^0, at 225 K under different stresses. The magnitude of the alignment stress is given in the figure.

was accomplished by holding the annealing temperature at 210 K and varying the stress between −0.20 and −0.45 GPa. Characteristic alignment times τ were recorded with the stress applied along both ⟨100⟩ and ⟨111⟩ crystallographic directions. This procedure has been described elsewhere.[12] The ⟨100⟩ stress-dependent energy barrier for transformation between the slow to the fast emitting defects is given by

$$\Delta E_r(P) = \Delta E_0 + (\alpha_{100}^{r0} - \alpha_{100}^{s0})P, \tag{2}$$

whereas for ⟨111⟩ stress the transformation take place from the fast to the slow emitting defect, i.e.,

$$\Delta E_r(P) = \Delta E_0 + (\alpha_{111}^{r0} - \alpha_{111}^{f0})P, \tag{3}$$

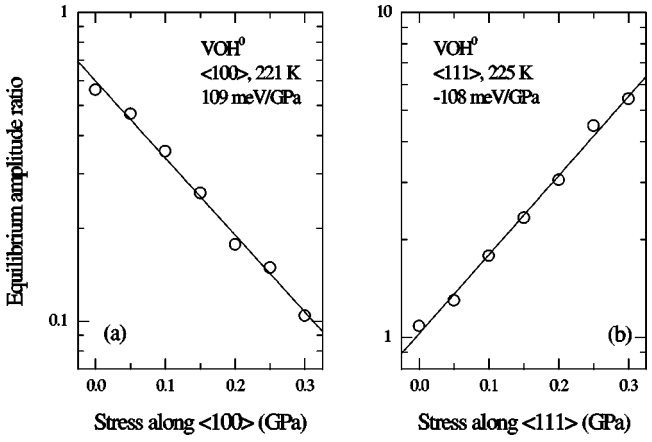

FIG. 8. Equilibrium amplitude ratio of the low-frequency to the high-frequency lines versus alignment stress applied to the neutral defect *V*OH^0 along (a) the ⟨100⟩ direction at 221 K and (b) the ⟨111⟩ direction at 225 K. The strain coefficients are +109 meV/GPa for the ⟨100⟩ stress direction and −108 meV/GPa for the ⟨111⟩ stress direction.

where α_t^{r0}, α_t^{s0}, and α_t^{f0} are strain coefficients for *V*OH^0 at the saddle point, *s* and *f* alignments, respectively, and ΔE_0 is the zero-stress barrier. Accordingly, we obtain strain coefficients of $\alpha_{100}^{r0} - \alpha_{100}^{s0} = 106$ meV/GPa and $\alpha_{111}^{r0} - \alpha_{111}^{f0} = 166$ meV/GPa. That means that the energy barrier the defect must overcome for reorientation decreases with compressive stress. An extrapolation of the energy barrier to zero stress gave $\Delta E_0 = 0.56$ eV.

IV. THEORETICAL MODELING

We use a local spin-polarized density-functional supercell method[22] (AIMPRO) with the Perdew-Wang exchange-correlation functional[23] and Bachelet-Hamann-Schlüter pseudopotentials.[24] The Kohn-Sham orbitals are expressed as linear combinations of *N* *sp*-like Cartesian-Gaussian atom-centered functions. For O, H, and Si, *N* is 6, 2, and 4, respectively. One set of *sp* functions is sited at the center of each bond formed between neighboring atoms. *V*OH defects were investigated by embedding them within otherwise perfect cubic supercells containing 64 Si atoms. The charge density and potential terms are expanded in plane waves with a 300 Ry energy cutoff, and the Brillouin zone is sampled with help of a Monkhorst-Pack MP-2^3 grid of special **k** points.[25] A detailed description of the method, including convergence issues, has been reported elsewhere.[11]

The electrical activity of *V*OH was studied according to the marker method.[26,27] Here, the location of donor (acceptor) level of defects is found by comparing their ionization energies (electron affinities) with those of a standard defect (the marker) with known electrical levels. This method is known to work best when the donor (acceptor) levels of the defect and marker are associated with wave functions with the same extent and symmetry. In this work, the *V*O defect[2] and the substitutional sulfur[28] defects (*V*O and S_s) are chosen as markers to determine the acceptor and donor levels, respectively. Six *s* and *p* Gaussian basis functions were placed on the sulfur species.

The reorientation barrier of the *V*OH complex was investigated by allowing the H and O atoms to move to new positions inside the vacancy. To explore the saddle point of the motion, we adopted a symmetry-constraint method, according to which a saddle point possessing distinct symmetry is relaxed while maintaining this symmetry. This enables the energies of structures lying midway between equivalent initial and final atomic configurations to be investigated. If the saddle point is perturbed by a slight atomic displacement, then the defect relaxes to the initial or final atomic configuration. This approach gives in general an upper bound for the reorientation barrier.

The piezospectroscopic response of the *V*OH defect is also calculated. The stress-energy tensor components are calculated by applying a set of deformations ϵ such that $B_{kl} = \partial E / \partial \epsilon_{kl}$, where E is the energy of the strained supercell. Care must be taken in order to make sure that all irreducible special **k** points are used as the symmetry of the problem may vary with ϵ. The change of energy with volume of a crystal containing a uniform concentration of defects is of course related to the ambient pressure. If this pressure is

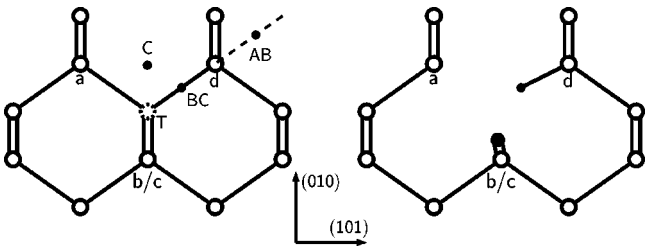

FIG. 9. The *V*OH complex (right). Projection of the diamond lattice showing high-symmetry sites of interest (left). Si, O, and H atoms are represented as open, large closed, and small closed circles, respectively. Dashed circle at the center of the bulk region represents a Si vacant site.

negligible then to first order $\mathrm{Tr}B^q=0$ and the stress tensor is traceless. This condition is satisfied by relaxing the volume of the unit cell in different charge states. It is possible to measure the change in volume of the defect consequent upon a change in charge state and isothermal DLTS measurements made under pressure have been carried out in some cases.[29] The evaluation of stress tensors of a number of defects have been reported previously for both Si[30–32] and diamond.[33]

Here, we focus on *V*OH structures possessing a twofold and threefold coordinated O atom *inside* the vacancy. These are the only low-energy forms that we found for the defect. On the left hand side of Fig. 9 we show a $(10\bar{1})$ projection of the diamond lattice. At the center lies a vacant site represented as a dashed circle. *V*OH defects are labeled according to their point symmetry. The trigonal (C_{3v}) structure possesses a threefold coordinated O atom near the *T* site and displaced along the $[\bar{1}\bar{1}1]$ direction, bridging Si_a, Si_b, and Si_c atoms in Fig. 9. On the other hand, monoclinic-I (C_{1h}) and orthorhombic-I (C_{2v}) structures possess a twofold coordinated O atom displaced along $[0\bar{1}0]$ away from the vacant site (see Fig. 9). All atoms in the supercell were allowed to relax until the resulting forces were smaller than 0.03 eV/Å.

Relative energies and structural details of the fully relaxed defects are shown in Table I. In line with our previous report,[11] we conclude that the C_{1h} structure is the ground state for the neutral and charged defects. This defect is shown on the right-hand side of Fig. 9, and it is formed by a vacancy with three of its Si dangling bonds saturated by O and H atoms. The H atom is bound to *V*O by $E_b=2.02$ eV,[11] where we considered isolated neutral bond-centered H and *V*O defects. To be compared to the measured dissociation energy (~ 2 eV), E_b has to be added to at least ~ 0.2 eV corresponding to the migration barrier of H. A similar overestimation has been found previously in other chalcogen-hydrogen complexes in Si.[27]

TABLE I. Relative energies (eV) and structural details (bond lengths in Å), of several *V*OH defect structures. Atom labeling is according to Fig. 9. Energies for the three charge states of interest are given.

Structure	C_{1h}	C_{2v}	C_{3v}
$E(+)$	0.00	0.08	0.14
$E(0)$	0.00	0.11	0.42
$E(-)$	0.00	0.18	0.72
$\mathrm{Si_b}$-O	1.694	1.689	1.926
$\mathrm{Si_d}$-H	1.512	1.795	1.493
$\mathrm{Si_a}$-H	2.656	1.795	2.772

The electrical activity emanates from the remaining Si dangling bond. The $\mathrm{Si_b}$-O ($\mathrm{Si_c}$-O) and $\mathrm{Si_d}$-H bond lengths are comparable with other defects with similar structural units. These include the *V*O and $V\mathrm{OH_2}$ complexes in Si.[4,11,34] The 2.7 Å distance between H and the Si_a dangling bond compares well with the 2.5 Å measured from the anisotropic component of the hyperfine tensor associated with the proton.[9]

A. Electrical levels

Using the electron affinity of *V*O as a marker, we place the acceptor level of *V*OH at $E_c-0.31$ eV, in agreement with the experimental level at $E_c-0.31$ eV. Similarly, using the ionization energy of S_s as a marker, we find the donor level of *V*OH at $E_v+0.35$ eV, again in agreement with the measured hole trap at $E_v+0.26$ eV. In this case the method has given energy levels at variance with the experiments by less than 0.1 eV, but in general errors as large as 0.2 eV can occur.

It is instructive to compare the *V*OH complex with the other chalcogen-hydrogen defects (S-H, Se-H, and Te-H).[27] From a simple atom-size argument, we conclude that for the lighter chalcogens, H tends to form a bond with Si at a bond-centered site, while for the heavier ones, antibonding Si-H units are favored. A *crossover* occurs in S-H, where two nearly degenerate bond-centered and antibonding configurations were found.[27,35] The Si_a dangling bond in *V*OH is responsible for the appearance of deep gap levels. This is not the case of the chalcogen-hydrogen complexes. Here only shallow donor activity was found due to threefold coordinated chalcogen atoms.

B. Stress-tensor calculations

We label each Si atom bordering the vacancy by the four letters a, b, c, and d [see Fig. 9(a)]. The 12 inequivalent orientations of the *V*OH(C_{1h}) defect can then be specified by ab, ac, ad, bc, bd, and cd, together with the six permuted combinations. Here, for example, da stands for a *V*OH defect with the H atom bonded to d and a dangling bond resides at a as shown in Fig. 9. In this orientation, the O atom bridges b and c, and the mirror plane is defined by d, a, and the T_d substitutional site. In some cases, da and ad may be equivalent under stress, and both orientations are then denoted by $\overline{ad}$.

The components of the B tensor are found as described at the beginning of Sec. IV, and those for *V*OH in all three charge states are given in Table II. Also shown for comparison are the measured stress tensor components of neutral *V*O in the same axial system. These immediately show that like *V*O,[2,11] the *V*OH complex is compressive along the [010] crystallographic direction (see Fig. 9), although *V*O shows a

TABLE II. Calculated stress-energy tensor components (eV) B_{kl} for VO^0, the da alignment of VOH (C_{1h}) (see Fig. 9), and d alignment of neutral VOH (C_{3v}). Components along $[10\bar{1}]$ and $[101]$ directions are also shown.

Structure	VO		VOH (C_{1h})		VOH (C_{3v})
Charge	0	−	0	+	0
B_{xx}	5.0	2.45	3.24	3.11	6.28
B_{yy}	−9.8	−4.90	−6.48	−6.22	6.28
B_{zz}	5.0	2.45	3.24	3.11	6.28
B_{xy}	0	−0.34	−1.63	−3.13	−7.62
B_{xz}	0.5	−7.21	−5.17	−4.63	−7.62
B_{yz}	0	−0.34	−1.63	−3.13	−7.62
$B_{10\bar{1}}$	5.5	9.66	8.41	7.74	
B_{101}	4.5	−4.76	−1.93	−1.52	

[a]Reference 11.

greater anisotropy as shown by its larger B_{yy} component. The component $B_{10\bar{1}}$ in Table II is similar to the dominant tensile Si-O-Si unit with $B_{10\bar{1}}\sim 8$ eV. This value is about 2 eV larger than that found in VO. Finally, the traceless condition makes VOH compressive along [101] in all charge states. It is interesting to note that the pronounced axial character of VO arises from the presence of the Si-Si tensile reconstruction. For VO we have $B_{101}=4.5$ eV. Once this bond is broken due to the presence of H, the [101] tensile strain is released along [010] and $[10\bar{1}]$ making the B_{yy} component for VOH smaller by about ~ 3.5 eV, and $B_{10\bar{1}}$ more tensile by ~ 3 eV.

Energy shifts Δ_t^{iq} for the various alignments for a particular stress direction can now be obtained by the use of Eq. (1). These are shown schematically in the configuration energy curves in Fig. 10 for a compressive stress with $P=-1$ GPa. Strain coefficients are readily obtained as $\alpha_t^{iq}=\Delta_t^{iq}/P$. As expected for C_{1h} symmetry, there are 2, 3, and 4 nonequivalent orientations for [100], [111], and [110] stresses, respectively.[19] The minima in the figure correspond to the 12 orientations of VOH and VOH$^-$ under different stresses. The barriers linking the minima are schematic and not all have been calculated (see below). The figure shows which orientations, e.g., $\overline{ac}$, $\overline{ad}$, $\overline{bc}$, and $\overline{bd}$, are degenerate under [100] stress and records the respective energy shifts Δ_t^{iq}. Thus for VOH$^-$, Δ_{100}^{ac-}, and Δ_{100}^{ab-} are -24 and $+48$ meV, respectively. The upper curves give the same information for the neutral charge state. This time Δ_{100}^{ac0} and Δ_{100}^{ab0} are -32 and $+64$ meV, respectively.

It is important to remember that the energy of the conduction electron e^- has to be added to the upper curve and enters the difference in the energies of VOH^0 and VOH$^-$ needed to obtain the ionization energy of the defect. Thus from the figure, compressive stress is seen to decrease the ionization energy of the $\overline{ac}$ population at a rate 32–24 or 8 meV/GPa and to increase the ionization energy of the $\overline{ab}$ population at a rate 64–48 or 16 meV/GPa, although the shift of the conduction band has to be added to both these figures. Nevertheless, we can say that the $\overline{ac}$ population is responsible for the fast, or high-frequency, transition and the $\overline{ab}$ population is responsible for the slow, or low-frequency

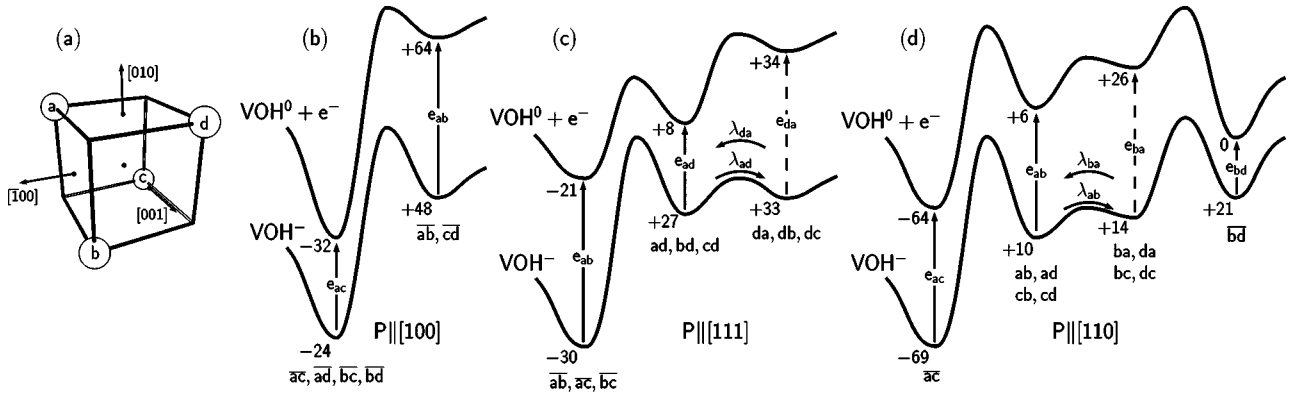

FIG. 10. In (a), we show our labeling scheme for the 12 different orientations of a C_{1h}-symmetry defect in a cubic crystal. Each orientation is labeled by an ordered letter pair denoting the site of H and the Si dangling bond (see text). In (b)–(d) we show schematic configuration coordinate diagrams for the defect under $P=-1$ GPa stresses along [100], [111], and [110], respectively, in the various orientations of the defect. Energy shifts Δ_t^{iq} (in meV) for all orientations are shown. Rates λ for the reorientation of H and emission rates e_i are represented by arrows.

one. The contribution by the shift in the conduction band prevents us from determining the shift of the level with stress, but the conduction-band energy does not enter into the expression for the level splitting. Consequently, the level splitting as shown in Fig. 10 is the difference between the ionization energies of the fast and slow populations and is calculated to be 24 meV/GPa and comparable with the observed value of 21 meV/GPa discussed earlier.

Let us now consider the amplitudes of the DLTS peaks. For random alignment, we expect the amplitude ratio for the low-frequency to the high-frequency component to be 4:8 arising from the population of $\overline{ab}$ and $\overline{cd}$ for the former and $\overline{ac}$, $\overline{ad}$, $\overline{bc}$, and $\overline{bd}$, for the latter. This agrees with the experimental result in Fig. 4. For alignment, Fig. 10 shows that the energy of the $\overline{ab}$ and $\overline{cd}$ populations (slow transition) increases relative to the other population at a rate 64 $+32$ or $+96$ meV/GPa. Thus the population giving the slow transition decreases, in agreement with the data, and the calculated strain coefficient is in close agreement with the observed one at $+109$ meV/GPa. Hence for [100] stress the theory is in very good agreement with the data.

We now consider [111] stress. Here we expect the C_{1h} symmetry to lead to *three* split components or three populations of defects. However, only two are detected. We suppose that this is because during the measurement cycle the defect switches between two orientations. We shall show below that the barrier for H jumping in the neutral *V*OH is very small. Now the difference between the atomic [Fig. 10(c)] structure of the ad, bd, and cd orientations on one hand, and da, db, and dc on the other in Fig. 10(c), is simply that the H atom has jumped to the other Si dangling bond. Thus, if the rates denoted by λ in Fig. 10(c) are much faster than the ionization rates (denoted by e_{da} and e_{ad}), then when the center is in one of these two families of orientations, it is able to switch to the other family very quickly until the defect emits an electron. Now, the ionization energy for the ad, bd, and cd orientations decreases with stress unlike that for the da, db, and dc orientations, and hence we expect that the observed transition out of these six orientations will take place for ad, bd, and cd. The ionization energy for the ad, bd, and $\overline{cd}$ population shifts by -19 meV/GPa while that for $\overline{ab}$, $\overline{ac}$, and $\overline{bc}$, it shifts by $+9$ meV/GPa (again neglecting the shift of the conduction band). Thus the slow component comes from the $\overline{ab}$, $\overline{ac}$, and $\overline{bc}$ population, whereas the fast one arises from the other populations. The relative splitting of the two levels will correspond to ~ 28 meV/GPa, in reasonable agreement with the observed value of 36 meV/GPa.

We now consider the amplitudes of the DLTS lines for the neutral defect. Here, the combined population of ad, bd, and cd defects, together with da, db, and dc, and responsible for the fast transition, equals the population of $\overline{ab}$, $\overline{ac}$, and $\overline{bc}$ responsible for the slow transition. Thus, in agreement with the observations for random orientations, we get an intensity ratio of 1:1. For alignment, we expect the population responsible for the slow transition to increase with stress at the expense of the other populations. This is in qualitative agreement with Fig. 8, however, the calculated strain coefficient of -29 meV/GPa is in poor agreement with the observed value of -108 meV/GPa. It seems that far fewer defects inhabit the higher-energy orientations. However, stress along $\langle 111 \rangle$ strongly reduces the reorientation barrier and this may mean that during the cooling process with stress on, the higher-energy defects reorientate increasing the population of lower-energy ones.

We finally consider the effect of [110] stress. Here, four levels are expected but, once again, only two are seen. Once again we anticipate that the H atom can rapidly jump between the two Si atoms and the two populations ab, ad, cb, cd and the permuted symbols lead to the same transition. The observed one will correspond to the faster transition given by the ab, ad, cb, cd orientations whose ionization energy decreases with stress. Thus three levels are anticipated. However, the ionization energy shifts of $\overline{ac}$, at 5 meV/GPa, and the ab, ad, cb, cd populations at -4 meV/GPa, are quite close and very different from the $\overline{bd}$ orientations at -21 meV/GPa. We then suppose that the levels of the $\overline{ac}$ and ab, ad, cb, cd populations cannot be resolved. The $\overline{bd}$ population leads to the fast transition and the others (ab, ad, cb, cd, ba, da, bc, dc, and $\overline{ac}$) are together responsible for the single slow transition. The level splitting rate of ~ 21 meV/GPa is in agreement with the experimental value of about 20 meV/GPa. The slow:fast ratio of intensities in the random case would be 10:2, and this agrees with the ratio shown in Fig. 4.

C. Reorientation of the *V*OH complex

It is clear that the rapid reorientation of the H atom is a key to understanding the stress Laplace DLTS experiment. Table I provides estimates of the adiabatic reorientation barriers in the three charge states. To achieve C_{2v} symmetry, the H atom jumps between Si dangling bonds with an adiabatic barrier of ~ 0.1–0.2 eV. The difference between the zero-point energies of the Si-H bonds at the stable and saddle-point configurations should be added. The vibrational frequencies certainly decrease in the C_{2v} state and if we suppose a reduction of 50%, we obtain a barrier *lowering* of about 0.05 eV from the Si-H stretch mode alone. The low barrier is consistent with EPR data giving an experimental value of 0.18 eV.

The barrier for both O and H reorienting, giving an averaged T_d symmetry, is estimated from the energy of the C_{3v} structure when O and H lie on a [111] axis. This is only 0.14 eV for $V\mathrm{OH}^+$, implying an ease for reorientation at low temperatures, and consistent with the lack of any stress splitting of the $E_v + 0.26$ eV donor level associated with the defect at 135 K (see Fig. 6). For $V\mathrm{OH}^0$, the barrier is 0.42 eV, in good agreement with the 0.56-eV barrier obtained from the stress-alignment experiments, while the barrier for $V\mathrm{OH}^-$ is larger, consistent with the difficulty of obtaining defect alignment in the negative charge state.

We now consider the effect of stress on the reorientation barrier of the O atom. Here we made two assumptions—(i) the saddle point is the C_{3v} configuration, and (ii) during reorientation the volume of the crystal does not change. This implies that the B tensor of the saddle point has a nonzero

trace, and this was calculated using a supercell with a lattice parameter corresponding to the volume-relaxed cell containing the C_{1h} form. A saddle-point alignment is labeled here with the character corresponding to the Si atom bonded to the H atom. For example, under [111] compressive stress, transformations $ad \rightarrow ac$ or $ad \rightarrow ab$ occur through a common saddle point *a* possessing a Si_a-H unit along $[1\bar{1}\bar{1}]$ (see Fig. 10).

The stress tensor components for the *d* alignment of the C_{3v} form are given in the rightmost column of Table II. We note that $\mathrm{Tr}(B) > 0$, meaning that it is a tensile state, and any $\langle 100 \rangle$ compressive stress will lower its energy. The off-diagonal components are negative, and whereas a [111] stress will increase the energy of the *d* state, it will lower the energy of the *a*, *b*, and *c* configurations. The calculated strain coefficients for the C_{3v} form are $\alpha_{100}^{a0} = +21$ meV/GPa, $\alpha_{111}^{a0} = +53$ meV/GPa, and $\alpha_{111}^{d0} = -74$ meV/GPa. In practical terms, this means that the barrier mediating the $ab^0 \rightarrow ac^0$ reorientation will change at a rate of $\alpha_{100}^{a0} - \alpha_{100}^{ab0} = +85$ meV/GPa under [100] stress. This is fairly close to the measured $\alpha_{100}^{r0} - \alpha_{100}^{s0} = +106$ meV/GPa. For [111] stress we predict an overall barrier change of $\alpha_{111}^{a0} - \alpha_{111}^{ad0} = +61$ meV/GPa. This is almost one-third of the measured value. This discrepancy is in line with that found for stress alignment. We also note that a similar softening of the reorientation barrier under stress was found for VO^0.[12] Accordingly, under $\langle 100 \rangle$ stress, the barrier was found to decrease by 84 meV/GPa, suggesting a similar bonding character of the O atom in both defects.

V. CONCLUSIONS AND DISCUSSION

We have shown that the annealing of the DLTS acceptor level at $E_c - 0.31$ eV coincides with the annealing of the EPR center attributed to *V*OH, and this fully confirms that the defects are identical. The experimental investigations using stress Laplace DLTS has shown that the acceptor level of *V*OH responds to $\langle 100 \rangle$, $\langle 111 \rangle$, and $\langle 110 \rangle$ stresses as a defect with an apparent C_{2v} symmetry, while the donor level at $E_v + 0.26$ eV is insensitive to stress, suggesting a T_d symmetry. The theory indicates that these are dynamic symmetries arising as a consequence of a rapid jump rate of the impurities within the vacancy cage. The true symmetry being C_{1h}, as indeed found in the low-temperature EPR study.[9] Quantitatively, the effect of $\langle 100 \rangle$ stress is completely understood: the calculations of both the magnitude of the stress splitting of the DLTS acceptor level into two components and the magnitude of the intensities of the DLTS lines both before and after reorientation of the defect agree well with experiment.

For $\langle 111 \rangle$ and $\langle 110 \rangle$ stresses, only two levels are found, whereas three and four are expected theoretically. However, the rapid H reorientation reduces the number of distinct levels by one and the coincidence in the strain coefficients for two of the distinct orientations of *V*OH under $\langle 110 \rangle$ stress reduces the number of resolvable transitions further. Qualitatively, the effect of $\langle 111 \rangle$ and $\langle 110 \rangle$ stresses is in agreement with the data but the magnitude of the alignment fraction for $\langle 111 \rangle$ stress is not reproduced.

Finally, we also report using DLTS a stress effect on the reorientation barrier of the defect. Compressive stress reduces the barrier. This effect has been confirmed by the theoretical calculation and is due to the closer separation of the saddle and initial configurations.

ACKNOWLEDGMENTS

Discussions with R. C. Newman and S. K. Estreicher and technical assistance of V. Kolkovski are acknowledged. This work has been supported in part by the State Committee for Scientific Research Grant No 4T11B02123 in Poland, the Danish National Research Foundation through the Aarhus Center for Atomic Physics (ACAP), and in the UK by the Engineering and Physical Science Research Council.

*Electronic address: coutinho@fis.ua.pt

†Present address: Topsil Semiconductor Materials, Linderupvej 4, 3600 Frederikssund, Denmark.

[1] G.D. Watkins, in *Deep Centers in Semiconductors*, 2nd ed., edited by S.T. Pantelides (Gordon and Breach, Switzerland, 1996), p. 177.

[2] G.D. Watkins and J.W. Corbett, Phys. Rev. **121**, 1001 (1961).

[3] B.G. Svensson and J.L. Lindström, Phys. Rev. B **34**, 8709 (1986).

[4] V.P. Markevich, L.I. Murin, M. Suezawa, J.L. Lindström, J. Coutinho, R. Jones, P.R. Briddon, and S. Öberg, Phys. Rev. B **61**, 12 964 (2000).

[5] K. Irmscher, H. Klose, and K. Maass, J. Phys. C **17**, 6317 (1984).

[6] A.R. Peaker, J.H. Evans-Freeman, P.Y.Y. Kan, L. Rubaldo, I.D. Hawkins, K.D. Vernon-Parry, and L. Dobaczewski, Physica B **273-274**, 243 (1999).

[7] K. Bonde Nielsen, L. Dobaczewski, K. Gościński, R. Bendesen, O. Andersen, and B. Bech Nielsen, Physica B **273-274**, 167 (1999).

[8] O. Feklisova, N. Yarykin, E.B. Yakimov, and J. Weber, Physica B **308-310**, 210 (2001).

[9] P. Johannesen, B. Bech Nielsen, and J.R. Byberg, Phys. Rev. B **61**, 4659 (2000).

[10] E. Artacho and F. Ynduráin, Solid State Commun. **72**, 393 (1989).

[11] J. Coutinho, R. Jones, P.R. Briddon, and S. Öberg, Phys. Rev. B **62**, 10 824 (2000).

[12] L. Dobaczewski, O. Andersen, L. Rubaldo, K. Gościński, V.P. Markevich, A.R. Peaker, and K. Bonde Nielsen, Phys. Rev. B **67**, 195204 (2003).

[13] L. Dobaczewski, P. Kaczor, I.D. Hawkins, and A.R. Peaker, J. Appl. Phys. **76**, 194 (1994).

[14] K. Bonde Nielsen, B. Bech Nielsen, J. Hansen, E. Andersen, and J.U. Andersen, Phys. Rev. B **60**, 1716 (1999).

[15] A.O. Evwaraye and E. Sun, J. Appl. Phys. **47**, 3776 (1976).

[16] S.D. Brotherton and P. Bradley, J. Appl. Phys. **53**, 5720 (1982).

[17] M.-A. Trauwaert, J. Vanhellemont, H.E. Maes, A.-M. Van Bavel, G. Langouche, and P. Clauws, Appl. Phys. Lett. **66**, 3056 (1995).

[18] P. Mooney, L.J. Cheng, M. Suli, J.D. Gerson, and J.W. Corbett, Phys. Rev. B **15**, 3836 (1977).

[19] A.A. Kaplyanskii, Opt. Spectrosc. **16**, 329 (1964).

[20] G.D. Watkins and J.W. Corbett, Phys. Rev. **138**, A543 (1965).
[21] G. D. Watkins, in *Early Stages of Oxygen Precipitation in Silicon*, Vol. 17 of *NATO Advanced Studies Institute, Series 3: High Technology*, edited by R. Jones (Kluwer Academic, Dordrecht, 1996), p. 1.
[22] P.R. Briddon and R. Jones, Phys. Status Solidi B **207**, 131 (2000).
[23] J.P. Perdew and Y. Wang, Phys. Rev. B **45**, 13 244 (1992).
[24] G.B. Bachelet, D.R. Hamann, and M. Schlüter, Phys. Rev. B **26**, 4199 (1982).
[25] H.J. Monkhorst and J.D. Pack, Phys. Rev. B **13**, 5188 (1976).
[26] A. Resende, R. Jones, S. Öberg, and P.R. Briddon, Phys. Rev. Lett. **82**, 2111 (1999).
[27] J. Coutinho, V.J.B. Torres, R. Jones, and P.R. Briddon, Phys. Rev. B **67**, 035205 (2003).
[28] H.G. Grimmeiss and E. Janzém, in *Deep Centers in Semiconductors*, 2nd ed., edited by S.T. Pantelides (Gordon and Breach, Switzerland, 1996), p. 97.
[29] G.A. Samara, Phys. Rev. B **36**, 4841 (1987).
[30] J. Coutinho, R. Jones, L.I. Murin, V.P. Markevich, J.L. Lindström, P.R. Briddon, and S. Öberg, Phys. Rev. Lett. **87**, 235501 (2001).
[31] J. Coutinho, R. Jones, P.R. Briddon, S. Öberg, L.I. Murin, V.P. Markevich, and J.L. Lindström, Phys. Rev. B **65**, 014109 (2002).
[32] O. Andersen, A.R. Peaker, L. Dobaczewski, K. Bonde Nielsen, B. Hourahine, R. Jones, P.R. Briddon, and S. Öberg, Phys. Rev. B **66**, 235205 (2002).
[33] J.P. Goss, R. Jones, and P.R. Briddon, Phys. Rev. B **65**, 035203 (2002).
[34] M. Pesola, J. von Boehm, T. Mattila, and R.M. Nieminen, Phys. Rev. B **60**, 11 449 (1999).
[35] I.S. Zevenbergen, T. Gregorkiewicz, and C.A.J. Ammerlaan, Phys. Rev. B **51**, 16 746 (1995).